

# Temperature variability is integrated by a spatially embedded decision-making center to break dormancy in Arabidopsis seeds

Topham, Alexander T.; Taylor, Rachel E.; Yan, Dawei; Nambara, Eiji; Johnston, Iain G.; Bassel, George W

DOI:

[10.1073/pnas.1704745114](https://doi.org/10.1073/pnas.1704745114)

License:

Other (please provide link to licence statement)

*Document Version*

Publisher's PDF, also known as Version of record

*Citation for published version (Harvard):*

Topham, AT, Taylor, RE, Yan, D, Nambara, E, Johnston, IG & Bassel, GW 2017, 'Temperature variability is integrated by a spatially embedded decision-making center to break dormancy in Arabidopsis seeds', *National Academy of Sciences. Proceedings*, vol. 114, no. 25, pp. 6629-6634. <https://doi.org/10.1073/pnas.1704745114>

[Link to publication on Research at Birmingham portal](#)

## General rights

Unless a licence is specified above, all rights (including copyright and moral rights) in this document are retained by the authors and/or the copyright holders. The express permission of the copyright holder must be obtained for any use of this material other than for purposes permitted by law.

- Users may freely distribute the URL that is used to identify this publication.
- Users may download and/or print one copy of the publication from the University of Birmingham research portal for the purpose of private study or non-commercial research.
- User may use extracts from the document in line with the concept of 'fair dealing' under the Copyright, Designs and Patents Act 1988 (?)
- Users may not further distribute the material nor use it for the purposes of commercial gain.

Where a licence is displayed above, please note the terms and conditions of the licence govern your use of this document.

When citing, please reference the published version.

## Take down policy

While the University of Birmingham exercises care and attention in making items available there are rare occasions when an item has been uploaded in error or has been deemed to be commercially or otherwise sensitive.

If you believe that this is the case for this document, please contact [UBIRA@lists.bham.ac.uk](mailto:UBIRA@lists.bham.ac.uk) providing details and we will remove access to the work immediately and investigate.

PNAS

PNAS

PNAS

PNAS

PNAS

PNAS

PNAS

PNAS

PNAS

PNAS

PNAS

PNAS

PNAS

PNAS

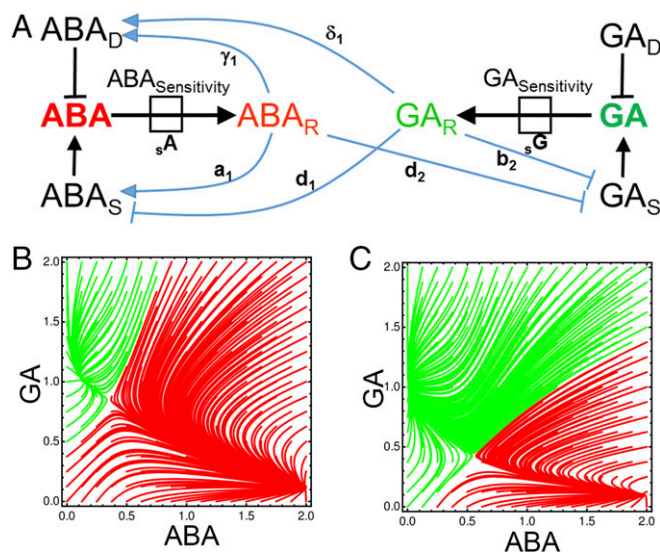
PNAS

PNAS

PNAS

PNAS

PNAS



these lines, including the position of the convergence points and threshold at which the system flips from one state to the other, is determined by the underlying ODEs and their parameterization.

Effective parameter sets for this model were identified harnessing a range of biological observations, and using approximate Bayesian computation with the criteria driving parameter selection was based on the similarity between simulated model behavior and observed biological behaviors (19) (*SI Appendix, Supplementary Materials and Methods*). The basin structure from inferred effective parameters yields a bifurcating output of relative hormone abundance in seeds, underlying bistable fate switching in this system (Fig. 1 *B* and *C*). These two outcomes are indicated by the presence of two different convergence points corresponding to a high-ABA, low-GA state and a high-GA, low-ABA state, representing the dormant and germinating states, respectively. Both deeply dormant (Fig. 1*B*) and less dormant (Fig. 1*C*) attractor basins are supported by the experimentally supported model. This shift to reduced dormancy is achieved by increasing the sensitivity of the system to GA (*SI Appendix, Supplementary Fig. 2*). The increase in GA sensitivity and *GID1* GA receptor abundance has been associated with the progressive loss of dormancy, such as during after ripening (20) or low-temperature treatment (18) (*SI Appendix, Supplementary Fig. 2*). The parameterized model also captures further observed responses to perturbations. Adding the ABA synthesis inhibitor norflurazon, or applying GA, is sufficient to stimulate germination in a portion of a dormant seed population (10) (*SI Appendix, Supplementary Fig. 3*), and these effects increase with the progressive loss of the depth of dormancy (21). These features are present in the less dormant model (Fig. 1*C*) and not the highly dormant model (Fig. 1*B*), whereby the

removal of ABA or addition of GA is sufficient to drive the system into the high-GA, low-ABA germination state. This dynamic model thus captures the bistable developmental fate switch in seeds, and recapitulates fate-switching observations following physiological and pharmacological interventions.

We next sought to understand how the spatial context of this decision-making module within the multicellular embryo body plan allows the plant to process environmental information. Genetically encoded components of GA and ABA synthesis, degradation, sensitivity, and response have been identified previously (4) (*SI Appendix, Supplementary Fig. 1 and Supplementary Table 1*). It has been established that germination is ultimately initiated within the *Arabidopsis* embryo and that this process is informed by the endosperm (10, 12, 21, 22). The cellular locations underlying this decision-making process remain unknown, however. Using 3D digital single-cell analysis, we localized ABA and GA hormone synthesis, degradation, and response reporter constructs in primary dormant embryos (23, 24) to reveal the cellular basis of decision making in seeds (Fig. 2 *A–I* and *SI Appendix, Supplementary Figs. 4–6*). All reporters investigated were enriched within the embryo radicle in primary dormant *Arabidopsis* seeds (*SI Appendix, Supplementary Figs. 4 and 5*). This result indicates that the subset of cells constituting the radicle constitutes a decision-making center within primary dormant *Arabidopsis* seeds.

The activity of the ABA-responsive *RAB18* promoter demonstrated the transcriptional response to this hormone to be localized to the outer cell layers of the embryo radicle, principally the root cap and epidermis (Fig. 2*A*). The promoter of the ABA response-promoting transcription factor *ABI3* was also found to be principally within the cells of the embryonic radicle (Fig. 2*B*), providing a spatial overlap between this upstream regulator and the final transcriptional output of the ABA pathway.

The cellular site of GA response was identified by characterizing the localization of the activity of the promoter of *SCL3*. This transcription factor stimulates GA responses, and the cellular localization of this promoter activity correlates with the accumulation of GA (25) and response to GA (26) in roots. The activity of the *SCL3* promoter was highly enriched within the vascular cells of the radicle (Fig. 2C), together with the GA receptors GID1A and GID1C, as well as DELLA proteins GAI and RGA (*SI Appendix, Supplementary Figs. 4 and 5*). These observations indicate that ABA and GA responses in nongerminating seeds occur within distinct cell types of the radicle, with the ABA response being enriched in the outer cells and the GA response within the inner cells, including the vasculature. This spatial separation of hormone responses suggests that cross-talk between ABA and GA is non-cell-autonomous and is controlled at the level of hormone movement between spatially separated signaling centers.

To understand how these distinct hormone response centers are spatially defined, we applied exogenous ABA and GA to primary dormant *RAB18::GUS* and *SCL3::GUS* seeds, respectively, to establish whether their patterns of activity were due to local hormone concentrations. Neither of these reporters showed appreciable ectopic induction in response to hormone application (*SI Appendix, Supplementary Fig. 7*), indicating that hormone response, and not local hormone abundance, defines the site of these signaling centers.

The spatial relationship between hormone metabolism and signaling was examined by localizing reporters to key synthesis and degradation components of these hormones. The penultimate step of ABA synthesis is catalyzed by ABA2, and the final step by AAO3. Both of these proteins were enriched within the outer cells of the radicle and within the vasculature of the radicle (Fig. 2*D* and *E*). CYP707A2 is the primary enzyme responsible for both ABA catabolism and seed dormancy breaking in *Arabidopsis* seeds (27). This protein is present as well within the root cap, epidermis, and vascular cells of the radicle in dormant embryos (Fig. 2*F* and *SI Appendix*, Supplementary Figs. 4 and 5). These localizations indicate that both ABA synthesis and degradation overlap with the distinct cellular response centers to ABA and GA.

The final step of GA synthesis is catalyzed by *GA 3-oxidase*, and GA degradation is mediated by *GA 2-oxidase*. Genes encoding



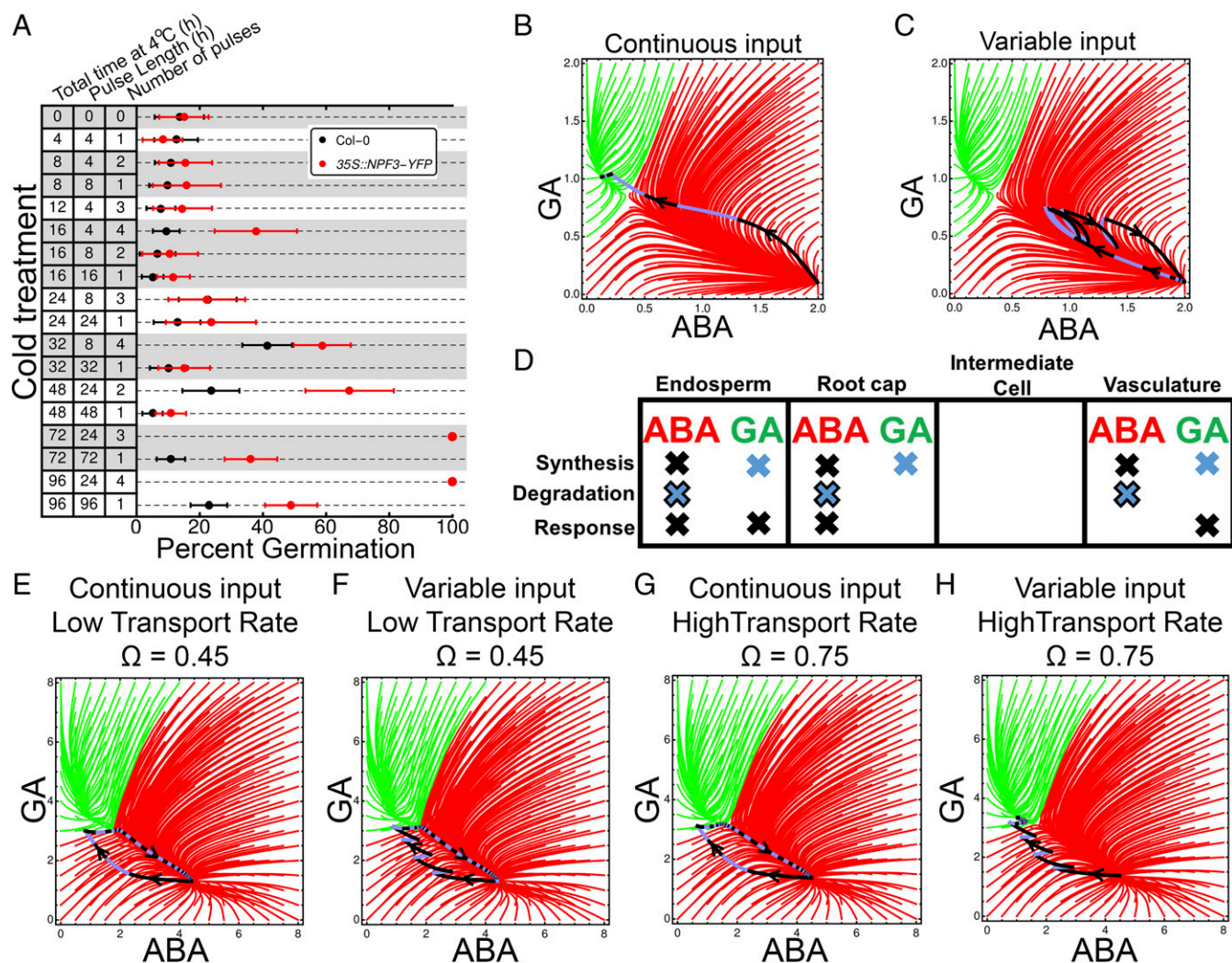


**Fig. 3.** Influence of interrupted cold treatment on developmental fate switching in dormant *Arabidopsis* seeds. (A) Percentage germination of wild-type Col-0 and 35S::NPF3-YFP seeds with continuous or interrupted cold (4 °C) for varying lengths of time, each counted 16 d after the start of the experiment. Single-region models with continuous virtual cold input (B) and interrupted cold input (C) are shown. (D) Schematic depicting the modeled distribution of metabolic components across the four-region model, motivated by our results on spatial localization of these components. Dark crosses indicate constitutively present components, pure blue crosses indicate components induced in response to cold (GA synthesis), and blue crosses with a dark outline represent constitutively present ABA degradation that is further induced in response to the cold (18). Dynamic behavior of the four-region model with continuous input and a low hormone transport rate (0.45) (E), variable input with a low hormone transport rate (F), continuous input and a high hormone transport rate (0.75) (G), and variable input and a high hormone transport rate (H) is illustrated. For the same total cold exposure, only a varying environment (sensed by communicating, separate compartments) breaks dormancy. Intervals of temperature treatment time in B, C, and E–H are indicated by different colors on the line drawn on the attractor basin, which depicts the trajectory of the system, alternating between black and blue, with each representing a single unit of time. Each continuous temperature and alternating temperature time unit is indicated using this same color scheme. Error bars in A indicate the 95% confidence interval.

The model indicated that if all processes are embedded in a single cell, continuous cold treatment is more effective than variable cold treatment in flipping the developmental fate switch following an equivalent length of low-temperature stimulus (Fig. 3B and C). To account for our observed spatial distribution of ABA and GA metabolic and response components across the various cell types of the radicle and the endosperm of dormant seeds, we extended our model to a multicell system, where four interconnected regions are endowed with the patterns of hormone synthesis, degradation, and response components established by microscopy (Fig. 3D) and signals are exchanged between these regions through a transport rate. A bistable switch is present within the four-compartment model as in the single-cell model (Fig. 3E and SI Appendix, Supplementary Materials and Methods and Supplementary Fig. 9). In light of the microarray data used to characterize interactions between hormone response and metabolic feedbacks being generated using whole

seeds, these relationships were still sufficient to generate the same output when spatially embedded. This model was also able to capture seed behavior dynamics following progressive dormancy loss through increases in GA sensitivity as observed in the single-cell model (SI Appendix, Supplementary Fig. 9), supporting the capacity of the multicell model to reflect observed seed behavior. Modifying hormone transport rates between different compartments did not drastically impact overall attractor basin architecture (SI Appendix, Supplementary Fig. 10).

The visual representation of this multidimensional system consisting of four cells and two hormones is limited in a single attractor basin 2D plot, which loses information. We note that, in some instances, this averaging can give the visual impression that a system has crossed over the threshold from one state to the other when, in the full phase space of the system, the threshold has not been passed.

When cell-to-cell communication is weak (lower transport rate), neither continuous (Fig. 3E) nor variable (Fig. 3F) cold stimuli were capable of flipping the dormancy fate switch. When cells communicated more readily (higher transport rates), continuous cold was incapable of flipping the switch (Fig. 3G), but, notably, a variable input did lead to the breaking of dormancy (Fig. 3H).

## Discussion

Here, the inferred nonlinear structure of interactions means that pulses of low-temperature stimulus and relaxation are more efficient at crossing the effective ABA/GA dynamic landscape than a single stimulus of the same total length. This behavior is analogous to the increased efficiency of evolutionary progress on complex landscapes under varying environments (39).

These observations indicate that the spatial separation of hormone metabolic interactions between communicating biological compartments provides the plant with a more efficient means of integrating variable temperature inputs into the flipping of the developmental fate switch. Additionally, increasing hormone transport rates further sensitizes the system to change fate in response to fluctuating inputs. To test this theory, we made use of a transgenic line overexpressing *NPF3*, a dual ABA and GA transporter (31), to examine what role increasing transport rates has on integrating variable inputs leading to fate switching in primary dormant *Arabidopsis* seeds. The *35S::NPF3* seeds showed a greater propensity to break dormancy in response to variable inputs than the wild-type control, as predicted by the model to a greater extent than in the response to continuous cold (Fig. 3A). The prediction of our model that increased hormone transport rates further sensitize seeds to low-temperature oscillations is thus verified within *Arabidopsis* seeds.

We have described a distributed signal and response system to ABA and GA in dormant seeds that contributes to sensing and responding to temperature variation. This spatial embedding of molecular components within multicellular architectures can therefore provide information-processing capacity that is absent without spatial structure. This observation is consistent with the increased computational capacities of cellular consortia over their unicellular counterparts (40), and can be likened to the principles of distributed computation. The joint exploitation of the geometry of a dynamical system and its nonlinear interactions supports decision making and the stepping of variable inputs toward effecting the flipping of a developmental fate switch in seeds. Although the topological configuration at the cellular level for decision making in *Arabidopsis* seeds is similar to the topological configuration at the cellular level for decision making in the human brain, the exploitation of this architecture is fundamentally different in the harnessing or filtering of inputs, respectively. The recognition of oscillations in temperature associated with soil depth and changing seasons may represent an important instructive clue toward ensuring accuracy in the timing and positioning of seedling establishment (41). Temperature oscillations in the soil are greatest at the surface and dampened with increased depth, and in the case of the small-seeded species *Arabidopsis*, the positioning of germination close to the top of the soil is as critical as timing it across the year. The short period of the temperature oscillations and responsiveness to these oscillations suggest that such daily stimuli plays an important role in this context. This mathematical and spatially embedded model provides a cellular and molecular template to understand and reengineer seed behavior in response to a changing environment.

## Materials and Methods

**Plant Growth Conditions.** To produce primary dormant seeds, seeds were germinated on 0.8% 1/2 MS agar, pH 6.2, after sterilization for 5 min in 10% bleach and rinsing with water. Once germinated, seedlings were transplanted to compost and grown in greenhouse conditions with 16-h days until plants had bolted. Plants were then transferred to a growth cabinet at a constant 12 °C, with 16-h white light cycles to produce primary dormant seeds (6).

**Generation of Transgenic Reporter Lines.** C-terminal GUS translational fusion lines for SLEEPY, RGA, GAI, and RGL2 were created by PCR amplification of the genomic region spanning from 2 kb upstream of the transcriptional start site until the final codon before the stop. The thymine residue of the stop codon was retained to keep the fragment in frame with the downstream protein fusion. This fragment was cloned into the GATEWAY entry vector pDNR221 and subcloned into GWB433, which contains a C-terminal GUS (42). The translational fusion of *CYP707A2::CYP707A2-GUS-3'* was obtained by overlap PCR using three fragments as templates. The first fragment is the *CYP707A2* genomic region, including the −1,887-bp upstream promoter region and the genomic region (excluding the stop codon); the second fragment is the GUS gene; and the third fragment is the 3' region covering the 1,989-bp genomic region downstream of the stop codon of *CYP707A2*. The overlap PCR product was cloned into entry vector pDONR207 and subcloned into binary vector pMDC99 (43).

**Seed Dormancy Sampling Conditions.** Primary dormant seeds were placed in 90-mm Petri dishes with three sheets of Fisherbrand filter paper (QL 100; Fisher) with sterile deionized water. Plates were placed at 22 °C in continuous white light. After 7 d, samples were dissected using a stereo binocular microscope, and embryo and endosperm samples were stained for GUS activity as described below.

**Hormone Application Treatment.** For hormone application with either GA or ABA (*SI Appendix, Supplementary Fig. 7*), primary dormant seeds were imbibed on water for 7 d and then transferred to plates containing 50 μM GA or 50 μM ABA. Samples were then collected, stained, and imaged at the times indicated.

**Dormancy Breaking Using GA and Norflurazon.** Primary dormant seeds were imbibed directly to 50 μM GA or 50 μM norflurazon, and their germination was counted after 13 d, either with or without the application of an initial cold treatment for 4 d at 4 °C (*SI Appendix, Supplementary Fig. 3*).

**Continuous and Interrupted Cold Treatment of Seeds.** Primary dormant seeds were imbibed on water and subjected to cold treatment at 4 °C for either continuous or interrupted intervals. Each cold interval took place within the duration of a 24-h time frame, either as 24 h of continuous cold, 4 h of cold, and 20 h at 22 °C or as 8 h of cold and 16 h at 22 °C. Cold treatment lasting 24 h was followed by a 24-h period at 22 °C. The total amount of time from when seeds were first imbibed until their final germination was counted was equal (16 d) for all samples.

**Statistical Analysis of Germination Data.** The 95% confidence intervals for the percentage of seeds germinated was calculated using

$$\hat{p} \pm z \sqrt{\frac{1}{n} \hat{p}(1-\hat{p})},$$

where  $\hat{p}$  is the proportion of germinated seeds,  $z$  is the  $1 - \frac{\alpha}{2}$  quantile of the standard normal distribution, and  $n$  is the number of seeds tested.

**Staining of Samples for Microscopy.** Dissected embryo samples were GUS-stained in X-Gluc solution consisting of 0.1 M sodium phosphate buffer (pH 7.0), 2 mM 0.1% Triton X-100, and X-Gluc for a variable time depending on the reporter used (32). Once the required level of GUS staining was attained, samples were fixed in a 3:1 solution of ethanol/acetic acid plus 500:1 DMSO, Tween 20, and Nonidet P-40 for at least 24 h. Following this treatment, cells were lysed in 0.2 N of sodium hydroxide + 1% SDS solution and kept at room temperature on a gyrotary platform until embryos turned translucent. If embryos did not turn fully translucent after this treatment, the fixing and lysis were repeated. After clearing, the embryos were incubated overnight at 37 °C in amylase to remove starch granules. After starch removal, aldehydes were produced by treating the embryos with 1% (wt/vol) periodic acid for 40 min, and cell walls could then be stained using 100 mM sodium metabisulfite in 0.15 N of HCl, mixed 9:1 with propidium iodide (44) until samples turned pink. After this final treatment, samples were cleared for at least 1 wk at a ratio of 4:1:2 by weight solution of chloral hydrate/glycerol/water.

Endosperm samples were fixed in the same way as embryos and then bleached using 25% (vol/vol) hypochlorite for 2 h to remove seed coat pigments. Samples were then mounted in Hoyer's medium on microscope slides and imaged on a Leica ICC50HD light microscope.

**Imaging and Computational Analysis of 3D Images.** Z-stacks of prepared samples were taken using an inverted Zeiss LSM710 laser-scanning confocal microscope. Samples were mounted in chloral hydrate solution (as described in the previous section) in glass-bottomed microscopy cell culture dishes (Greiner Bio One) using a 25× oil-immersion objective (LD LCI Plan-Apochromat 25×/0.8; Zeiss) and excited using an argon-ion laser. Cell wall (propidium iodide) signal was collected between 530-nm and 735-nm wavelengths, and GUS signal was collected as reflectance at between 483-nm and 493-nm wavelengths.

LSM files were then converted into tiled resulting tagged image file format (TIFF) images using Fiji (45), with separate stacks for the propidium iodide and GUS channels. The resulting TIFF images were then imported into MorphoGraphX (MGX) (23). Samples were subjected to a Gaussian image blur using a radius of 0.5, and then segmented using the auto-seeded watershed algorithm of the Insight Toolkit image-processing library. A typical threshold for the watershed was around 500, aiming to have no under-segmentation of any cells in the stack. Oversegmentation was then corrected manually, and the edited segmented stack was then used to generate a 3D mesh using the marching cubes algorithm in MGX, using a cube size of two and seven smoothing passes at the time of meshing. This mesh was then used for all downstream analyses.

For quantitative reporter concentration data, the stack containing the GUS channel was loaded into MGX along with the mesh. Using MGX's heat map

function, GUS concentration data could be obtained by reporting to a spreadsheet the "signal average" of the volumetric, "interior signal" data calculated from the mesh combined with the GUS reporter stack. For whole-axis heat maps, the same process was used. Here, images of the mesh with the heat map overlaid were taken from within MGX and exported as JPEG images. Heat maps were scaled such that the intensity of all visible cells ranged from zero (blue) to dark red.

Two-dimensional images were taken using the same Zeiss LSM710 setup, but limited to single optical sections. These images were used to highlight the distribution of reporters across the entire embryo.

**Lines Used and Quantification of GUS Activity.** The lines used in this study are listed in *SI Appendix, Supplementary Table 1*. GUS activity was quantified using the fluorometric assays described by Stamm et al. (46).

**ACKNOWLEDGMENTS.** We thank Harriet Davies for technical support. G.W.B. and A.T.T. were supported by Biotechnology and Biological Sciences Research Council (BBSRC) Grant BB/L010232/1, and G.W.B. was supported by BBSRC Grants BB/J017604/1 and BB/N009754/1. I.G.J. was supported by a Birmingham Fellowship. D.Y. and E.N. were funded by Natural Sciences and Engineering Research Council Discovery Grant RGPIN-2014-03621.

- Domagalska MA, Leyser O (2011) Signal integration in the control of shoot branching. *Nat Rev Mol Cell Biol* 12:211–221.
- Angel A, Song J, Dean C, Howard M (2011) A Polycomb-based switch underlying quantitative epigenetic memory. *Nature* 476:105–108.
- Boss PK, Bastow RM, Mylne JS, Dean C (2004) Multiple pathways in the decision to flower: Enabling, promoting, and resetting. *Plant Cell* 16(Suppl):S18–S31.
- Finch-Savage WE, Leubner-Metzger G (2006) Seed dormancy and the control of germination. *New Phytol* 171:501–523.
- Finch-Savage WE, Bassel GW (2016) Seed vigour and crop establishment: Extending performance beyond adaptation. *J Exp Bot* 67:567–591.
- Chiang GC, Barua D, Kramer EM, Amasino RM, Donohue K (2009) Major flowering time gene, flowering locus C, regulates seed germination in *Arabidopsis thaliana*. *Proc Natl Acad Sci USA* 106:11661–11666.
- Bentsink L, Jowett J, Hanhart CJ, Koornneef M (2006) Cloning of DOG1, a quantitative trait locus controlling seed dormancy in *Arabidopsis*. *Proc Natl Acad Sci USA* 103:17042–17047.
- Footitt S, Douterelo-Soler I, Clay H, Finch-Savage WE (2011) Dormancy cycling in *Arabidopsis* seeds is controlled by seasonally distinct hormone-signaling pathways. *Proc Natl Acad Sci USA* 108:20236–20241.
- Karssen CM, Brinkhorst-van der Swan DL, Breekland AE, Koornneef M (1983) Induction of dormancy during seed development by endogenous abscisic acid: Studies on abscisic acid deficient genotypes of *Arabidopsis thaliana* (L.) Heynh. *Planta* 157:158–165.
- Bradford KJ, Trewavas AJ (1994) Sensitivity thresholds and variable time scales in plant hormone action. *Plant Physiol* 105:1029–1036.
- Luckwill L (1953) Studies of fruit development in relation to plant hormones: I. Hormone production by the developing apple seed in relation to fruit drop. *J Hort Sci* 28:14–24.
- Bassel GW (2016) To grow or not to grow? *Trends Plant Sci* 21:498–505.
- Karssen C, Lacka E (1986) A revision of the hormone balance theory of seed dormancy: Studies on gibberellin and/or abscisic acid-deficient mutants of *Arabidopsis thaliana*. *Plant Growth Substances 1985, Proceedings in Life Sciences*, ed Bopp M, (Springer, Berlin), pp 315–323.
- Tyson JJ, Chen KC, Novak B (2003) Sniffers, buzzers, toggles and blinkers: Dynamics of regulatory and signaling pathways in the cell. *Curr Opin Cell Biol* 15:221–231.
- Artavanis-Tsakonas S, Rand MD, Lake RJ (1999) Notch signaling: Cell fate control and signal integration in development. *Science* 284:770–776.
- Seo M, et al. (2006) Regulation of hormone metabolism in *Arabidopsis* seeds: Phytochrome regulation of abscisic acid metabolism and abscisic acid regulation of gibberellin metabolism. *Plant J* 48:354–366.
- Ogawa M, et al. (2003) Gibberellin biosynthesis and response during *Arabidopsis* seed germination. *Plant Cell* 15:1591–1604.
- Yamauchi Y, et al. (2004) Activation of gibberellin biosynthesis and response pathways by low temperature during imbibition of *Arabidopsis thaliana* seeds. *Plant Cell* 16:367–378.
- Toni T, Stumpf MP (2010) Simulation-based model selection for dynamical systems in systems and population biology. *Bioinformatics* 26:104–110.
- Hauvermale AL, Tuttle KM, Takebayashi Y, Seo M, Steber CM (2015) Loss of *Arabidopsis thaliana* seed dormancy is associated with increased accumulation of the GID1 GA hormone receptors. *Plant Cell Physiol* 56:1773–1785.
- Debeaujon I, Koornneef M (2000) Gibberellin requirement for *Arabidopsis* seed germination is determined both by testa characteristics and embryonic abscisic acid. *Plant Physiol* 122:415–424.
- Lee KP, Piskurewicz U, Turecková V, Strnad M, Lopez-Molina L (2010) A seed coat bedding assay shows that RGL2-dependent release of abscisic acid by the endosperm controls embryo growth in *Arabidopsis* dormant seeds. *Proc Natl Acad Sci USA* 107:19108–19113.
- Barbier de Reuille P, et al. (2015) MorphoGraphX: A platform for quantifying morphogenesis in 4D. *eLife* 4:05864.
- Montenegro-Johnson TD, et al. (2015) Digital single-cell analysis of plant organ development using 3DCellAtlas. *Plant Cell* 27:1018–1033.
- Shani E, et al. (2013) Gibberellins accumulate in the elongating endodermal cells of *Arabidopsis* root. *Proc Natl Acad Sci USA* 110:4834–4839.
- Ubeda-Tomás S, et al. (2008) Root growth in *Arabidopsis* requires gibberellin/DELLA signalling in the endodermis. *Nat Cell Biol* 10:625–628.
- Okamoto M, et al. (2006) CYP707A1 and CYP707A2, which encode abscisic acid 8'-hydroxylases, are indispensable for proper control of seed dormancy and germination in *Arabidopsis*. *Plant Physiol* 141:97–107.
- Cadman CS, Toorop PE, Hilhorst HW, Finch-Savage WE (2006) Gene expression profiles of *Arabidopsis* Cvi seeds during dormancy cycling indicate a common underlying dormancy control mechanism. *Plant J* 46:805–822.
- Bassel GW, et al. (2008) Elucidating the germination transcriptional program using small molecules. *Plant Physiol* 147:143–155.
- Kanno Y, et al. (2012) Identification of an abscisic acid transporter by functional screening using the receptor complex as a sensor. *Proc Natl Acad Sci USA* 109:9653–9658.
- Tal I, et al. (2016) The *Arabidopsis* NPF3 protein is a GA transporter. *Nat Commun* 7:11486.
- Bassel GW, et al. (2014) Mechanical constraints imposed by 3D cellular geometry and arrangement modulate growth patterns in the *Arabidopsis* embryo. *Proc Natl Acad Sci USA* 111:8685–8690.
- Tsuchiya Y, et al. (2015) PARASITIC PLANTS. Probing strigolactone receptors in *Striga hermonthica* with fluorescence. *Science* 349:864–868.
- Bogacz R, Gurney K (2007) The basal ganglia and cortex implement optimal decision making between alternative actions. *Neural Comput* 19:442–477.
- Bogacz R (2007) Optimal decision-making theories: Linking neurobiology with behaviour. *Trends Cogn Sci* 11:118–125.
- Fitts PM (1954) The information capacity of the human motor system in controlling the amplitude of movement. *J Exp Psychol* 47:381–391.
- Morinaga T (1926) Effect of alternating temperatures upon the germination of seeds. *Am J Bot* 13:141–158.
- Angel A, et al. (2015) Vernalizing cold is registered digitally at FLC. *Proc Natl Acad Sci USA* 112:4146–4151.
- Kashtan N, Alon U (2005) Spontaneous evolution of modularity and network motifs. *Proc Natl Acad Sci USA* 102:13773–13778.
- Regot S, et al. (2011) Distributed biological computation with multicellular engineered networks. *Nature* 469:207–211.
- Thompson K, Grime JP, Mason G (1977) Seed germination in response to diurnal fluctuations of temperature. *Nature* 267:147–149.
- Nakagawa T, et al. (2007) Improved Gateway binary vectors: High-performance vectors for creation of fusion constructs in transgenic analysis of plants. *Biosci Biotechnol Biochem* 71:2095–2100.
- Curtis MD, Grossniklaus U (2003) A gateway cloning vector set for high-throughput functional analysis of genes in plants. *Plant Physiol* 133:462–469.
- Truernit E, et al. (2008) High-resolution whole-mount imaging of three-dimensional tissue organization and gene expression enables the study of Phloem development and structure in *Arabidopsis*. *Plant Cell* 20:1494–1503.
- Schindelin J, et al. (2012) Fiji: An open-source platform for biological-image analysis. *Nat Methods* 9:676–682.
- Stamm P, et al. (2017) The transcription factor ATHB5 affects GA-mediated plasticity in hypocotyl cell growth during seed germination. *Plant Physiol* 173:907–917.
- Nakabayashi K, Okamoto M, Koshida T, Kamiya Y, Nambara E (2005) Genome-wide profiling of stored mRNA in *Arabidopsis thaliana* seed germination: Epigenetic and genetic regulation of transcription in seed. *Plant J* 41:697–709.